Versatile fabrication of aligned SnO$_2$ nanotube arrays by using various ZnO arrays as sacrificial templates†‡

Qin Kuang, Tao Xu, Zhao-Xiong Xie,* Shui-Chao Lin, Rong-Bin Huang and Lan-Sun Zheng

In this paper, we describe an effective two-step method for fabricating aligned SnO$_2$ nanotube arrays by using various pre-synthesized ZnO nanorod arrays as sacrificial templates. The composition and structure of as-synthesized SnO$_2$ nanotube arrays were analyzed in detail by X-ray diffraction, scanning electron microscopy, and transmission electron microscopy. Because there is a special epitaxial relation between the SnO$_2$ walls and ZnO templates, the walls building the SnO$_2$ nanotubes are highly orientated and nearly single-crystalline. Our present study provides an opportunity to investigate related physical and chemical properties and potential applications of such aligned SnO$_2$ nanotubes with nearly single-crystalline nature.

Introduction

Recently, tubular inorganic nanomaterials have attracted great interest as a result of their unique structures and potential applications in catalyst, drug delivery, separation system and so on.[1–5] Up to now, various synthetic strategies have been developed to fabricate inorganic nanotubes, based on the self-curling mechanism,[6,7] Kirkendall effect,[8] template-directed synthesis,[9–12] etc. Among these strategies, the template-directed synthesis is the most popular method for the synthesis of tubular inorganic nanomaterials. For this kind of strategy, various one-dimensional (1D) nanostructures including porous materials,[9,10] cylindrical micelles,[11] and nanowires,[12] have been applied as templates to direct the formation of tubular nanomaterials, followed by selective removal of the templates.[13] In comparison with other synthetic strategies, the template-directed route is more facile and controllable.

Tin oxide (SnO$_2$), an *n*-type semiconductor with a wide bandgap (E_g = 3.6 eV, 300 K), possesses remarkable receptivity variation in gaseous environment, high optical transparency in the visible range (up to 97%), low resistivity (10^{-4}–10^6 $\Omega \cdot cm^{-1}$) and excellent chemical stability. As a result, SnO$_2$ is widely used in chemical sensors, dye-sensitized solar cells and transparent conductors.[14–17] Previous studies have demonstrated that tubular SnO$_2$ nanostructures exhibit higher capacity retention and better cyclability than common commercial anode materials for lithium-ion batteries.[15] At the same time, tubular SnO$_2$ nanostructures were found to exhibit high sensitivity and quick response time for detecting some combustible gases, such as

State Key Laboratory for Physical Chemistry of Solid Surfaces & Department of Chemistry, College of Chemistry and Chemical Engineering, Xiamen University, Xiamen, 361005, P.R. China. E-mail: zxxie@xmu.edu.cn; Fax: +86-592-2183047; Tel: +86-592-2180627

† This paper is part of a *Journal of Materials Chemistry* theme issue on Nanotubes and Nanowires. Guest editor: Z. L. Wang.
‡ Electronic supplementary information (ESI) available: High-magnification side-view SEM image of as-synthesized SnO$_2$ nanotube array by templating rod-like ZnO array, XRD patterns of SnO$_2$ nanotubes obtained from rod-like ZnO arrays after deposition times of 2 min and 15 min. See DOI: 10.1039/b815514c

ethanol, ammonia and H$_2$.[16c,d] To date, most tubular SnO$_2$ nanostructures are obtained *via* sol–gel or electrophoretic processing combined with various porous membranes including anodic aluminium oxide, polycarbonate and mesoporous silica.[15,16c,d,18,19] However, the SnO$_2$ nanotubes prepared by the above-mentioned methods are always polycrystalline and composed of random nanoparticles. Furthermore, those SnO$_2$ nanotubes are freestanding, and very difficult to be directly used in nanodevices because they cannot arrange in an ordered fashion on the solid surface after the removal of the templates. Therefore, continuous efforts are still required to find a facile and versatile synthetic method to obtain aligned single-crystalline SnO$_2$ nanotubes. Sacrificial template synthesis based on epitaxial core/shell heterostructures, which is also called an epitaxial casting approach in some references,[20–22] is a feasible route to realize this purpose. For example, single-crystalline GaN nanotube arrays have been successfully fabricated by using aligned ZnO nanowires as removable templates.[21] Some previous studies have demonstrated that rutile-type SnO$_2$ and wurtzite-type ZnO have a special epitaxial relationship,[23] and their acid resistance abilities are distinct, which provides a possible pathway to obtain aligned single-crystalline SnO$_2$ nanotubes by an epitaxial casting approach.

Inspired by this idea, we propose an effective two-step method for fabricating aligned SnO$_2$ nanotube arrays by using various pre-synthesized ZnO arrays as sacrificial templates. The best advantage of our strategy is the easy tuning of the construction form and the wall thickness of SnO$_2$ nanotube walls by selecting various ZnO arrays with different diameters and controlling the experimental conditions of SnO$_2$ deposition. Our experiments demonstrate that the walls of as-synthesized SnO$_2$ nanotubes are highly orientated and nearly single-crystalline.
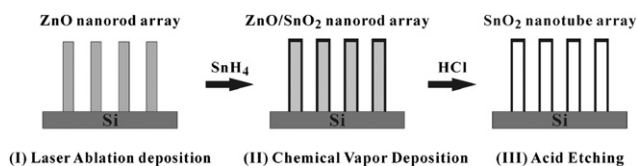
Experimental

Syntheses of SnO$_2$ nanotube arrays

Scheme 1 shows a schematic illustration of the fabrication process for aligned SnO$_2$ nanotube arrays by using various ZnO

This journal is © The Royal Society of Chemistry 2009

J. Mater. Chem., 2009, **19**, 1019–1023 | 1019

Scheme 1 Schematic illustration of the fabrication processes for aligned SnO$_2$ nanotube arrays by using various ZnO arrays as sacrificial templates.

arrays as sacrificial templates. A typical synthetic procedure was carried out as follows.

(1) Pre-synthesis of ZnO arrays. Various ZnO arrays used as sacrificial templates were prepared in advance by means of a laser-ablation deposition method, which refers to a technique reported previously in ref. 24 with a minor modification. During the deposition process, the deposition temperature of the Si substrate was kept about 600–750 °C and the laser-ablation process lasted 2–10 min. After reaction, a white film was deposited on the Si substate.

(2) Desposition of SnO$_2$ shell on ZnO arrays. In this step, as-obtained ZnO arrays were coated with a layer of SnO$_2$ shell *via* chemical vapor deposition (CVD) using SnH$_4$ as the precursor, which was carried out in a homemade CVD apparatus. The details of this experiment are similar to our previous work on epitaxial ZnO/SnO$_2$ core–shell tetrapods.[23a] In a typical experiment, after the reaction chamber was placed under vacuum, the Si substrate loading ZnO nanorod array was heated to 770 °C, and then SnH$_4$/N$_2$ mixed gas was introduced into the chamber at a flow rate of 10 sccm (standard cubic centimeter per minute). The deposition procedure lasted 2–15 min, and the pressure in the reaction chamber was kept about 23.2 torr during the whole procedure.

(3) Formation of aligned SnO$_2$ naotube arrays. In this step, ZnO/SnO$_2$ core–shell nanostructure arrays were converted into corresponding SnO$_2$ nanotube arrays by means of acid etching. In a typical experiment, as-prepared ZnO/SnO$_2$ core–shell nanostructure arrays together with the Si substrates were placed on a glass culture dish and then immersed in 0.1 M HCl solution for 30 min–2 hours. After that, the samples were transferred into clean water and left undisturbed for about 2 hours. Finally, the samples were dried under an infrared lamp.

Characterization of SnO$_2$ nanotube arrays

The composition of the products was confirmed by powder X-ray diffraction (XRD) pattern using a Panalytical X-pert diffractometer with copper Kα radiation. The morphology and crystal structure of the products were characterized by field emission scanning electron microscope (FE-SEM, LEO 1530) equipped with energy dispersion spectroscopy (EDS) and high-resolution TEM (HRTEM, Philips TECNAI F-30) with an acceleration voltage of 300 KV. For the XRD measurement, the as-synthesized SnO$_2$ nanotubes were carefully collected from the Si substrate. The specimens for TEM characterization were prepared by removing the SnO$_2$ nanotubes from the substrate to

ethanol solvent, and then dropping the ultrasonically dispersed ethanol suspensions on a carbon-coated copper grid and drying in air before analysis.

Results and discussion

The morphologies of pre-synthesized ZnO samples were first examined by SEM. Fig. 1a–c show typical SEM images of three kinds of ZnO array obtained by laser-ablation deposition at the temperature of 600 °C–750 °C. There are obvious differences between the shapes of these ZnO nanorods, and therefore we here define them as rod-like, column-like, and tower-like ZnO arrays for convenience. For the rod-like arrays, the diameters of ZnO nanorods are relatively uniform along the axial direction, ranging from 300 nm to 500 nm (Fig. 1a). Column-like ZnO have well-defined hexagonal cross-sections, and their diameters are about 1–1.5 μm (Fig. 1b). For the tower-like ZnO arrays, the diameters of ZnO decrease gradually from the root (about several μm) to the top (200 nm), and thus they look like towers (Fig. 1c). Despite their different diameters and shapes, all three types of ZnO nanorods are able to vertically align well over the entire Si substrates. Such good alignment of ZnO nanorods is further confirmed by their corresponding XRD analysis. As shown in Fig. 1d, the XRD pattern is dominated by a very sharp and strong (002) reflection of wurtzite-type ZnO at 34.4°, which indicates the strong c-axis alignment of as-synthesized ZnO nanorods.

The crystallinity of as-synthesized ZnO nanorods was further examined by TEM. As an example, Fig. 1e shows an individual ZnO nanorod with a diameter of about 360 nm. The
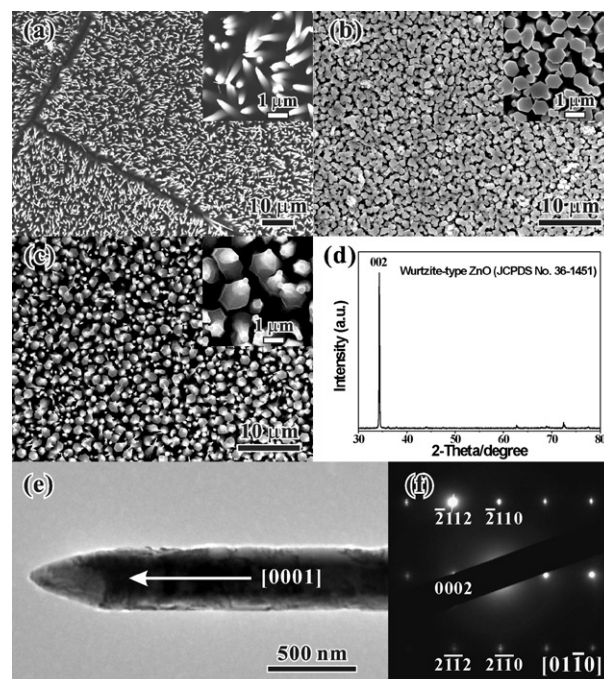

Fig. 1 Typical SEM images of various ZnO nanorod arrays with (a) rod-like, (b) column-like, and (c) tower-like shapes; the insets are corresponding high-magnification images. (d) Typical XRD pattern, (e) low-magnification TEM image, and (f) corresponding SAED pattern of the same sample as in (a).

corresponding selected area electron diffraction (SAED) pattern (Fig. 1f) can be identified as the [01$\bar{1}$0] zone axis projection of wurtzite-type ZnO. Perfect diffraction spots indicate that ZnO nanorods are single-crystalline and preferentially grow along the [0001] direction.

After the SnO_2 deposition and subsequent removal of templates, the film remains on the substrates, and the colour changes from white to grey. Fig. 2a–c show typical morphologies of the products prepared by using three types of ZnO arrays as the sacrificial templates. The corresponding XRD pattern and EDS spectrum confirm that these hollow tubular structures are pure SnO_2 of rutile structure, and ZnO nanorods as sacrificial templates have been thoroughly removed (Fig. 2d and e show the representative XRD pattern and EDS spectrum of SnO_2 nanotubes obtained by using rod-like ZnO templates). It can been clearly that all the products exhibit hollow structures standing vertically on the substrates. In particular, these hollow structures almost replicated the original morphologies of the ZnO templates no matter what the shape and size of the original ZnO templates. As shown in Fig. 2a, the SnO_2 nanotubes resulting from the rod-like ZnO array have inner diameters of 300–500 nm, consistent with the diameter of the initial ZnO nanorod templates, and their walls are very rough, about 60–90 nm in thickness. Most nanotubes (about 70%) exhibit closed ends. According to its high-magnification side-view image (see Fig. S1 in Electronic Supplementary Information (ESI)‡), the walls of the root portion of these nanotubes are not compact, made up of

numerous tiny particles, but the walls of the upper portion become a continuous film with a rough surface. For the walls of SnO_2 nanotubes resulting from column-like ZnO array, they are constructed with nanostructures (Fig. 2b) with an angle of 120°, which duplicate the hexagonal shape of ZnO columns.

In the case of the tower-like ZnO array template, the shape of the initial ZnO template was also directly reflected in the resulting SnO_2 nanotubes as show in Fig. 2c. It can be found that all SnO_2 nanotubes entirely duplicated the tower-like morphology of the initial ZnO templates. It should be noted that the construction forms of tubular walls are different with the variation of the diameters along the axial direction of the nanotubes. As shown in the partially enlarged image (the inset of Fig. 2c), the walls at the roots and the tops of these tower-like SnO_2 nanotubes are continuous films built by tiny particles, which is similar to those nanotubes obtained by using rod-like ZnO templates. At the middle of the nanotubes, however, some special stepped structures with uniform height of about 200 nm are clearly observed. Such stepped structures of the middle tubular walls are formed by stacking of some hexagons with gradually decreasing diameters along the axial direction of SnO_2 nanotubes.

To explore structural information of the walls of these SnO_2 nanotubes, the tower-like SnO_2 nanotubes as an representative example were dispersed onto a TEM grid for further structural analysis. Fig. 3a is a typical TEM image of the top of an individual tower-like SnO_2 nanotube. Clear lattice fringes for (100) planes of the rutile-type SnO_2 are resolved on its HRTEM image of the top surface (Fig. 3b). The corresponding SAED pattern (Fig. 3c) recorded from the whole nanotube show regular diffraction spots, which can be indexed as the [010] zone axis projection of rutile-type SnO_2. The above results indicate that the wall of the as-synthesized SnO_2 nanotube is highly orientated, and can be regarded as a nearly single-crystalline film. The axial direction of the SnO_2 nanotubes is along the [100] direction. Fig. 3d is a typical TEM image of the middle of the identical tower-like SnO_2 nanotube. As pointed by the arrows in the figure, some planar structural defects with nearly equal intervals
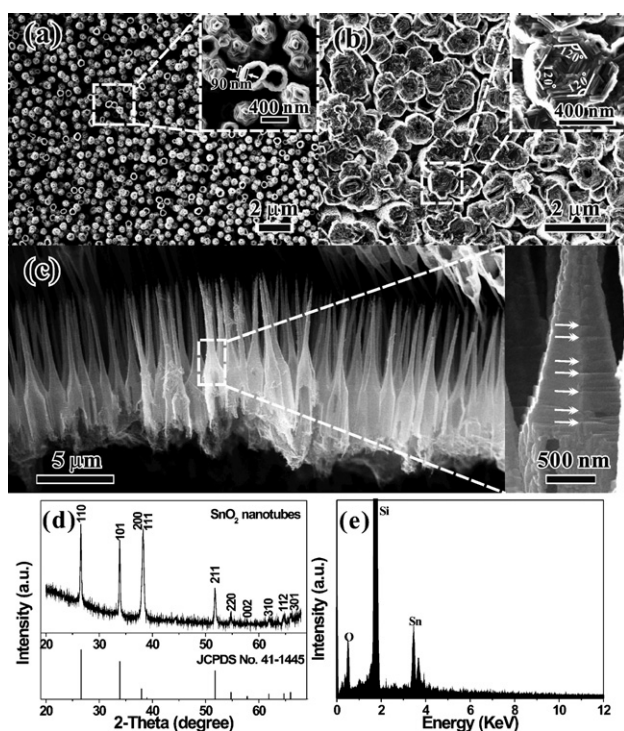

Fig. 2 Typical SEM images of vertically standing SnO_2 nanotubes prepared by using (a) rod-like, (b) column-like and (c) tower-like ZnO arrays as the sacrificial templates; The right insets are corresponding partially enlarged images. (d) XRD pattern and (e) EDS spectrum of SnO_2 nanotubes obtained by using rod-like ZnO arrays as the sacrificial template. The deposition time of SnO_2 was 10 min.
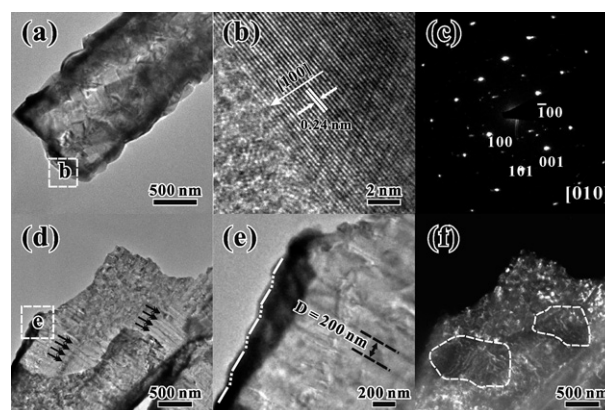

Fig. 3 (a) Low-magnification TEM image, (b) HRTEM image and (c) corresponding SAED pattern of an individual tower-like SnO_2 nanotube; (d) low-magnification TEM image, (e) partial enlarged image and (f) corresponding dark-field TEM image of the middle of the identical tower-like SnO_2 nanotube.
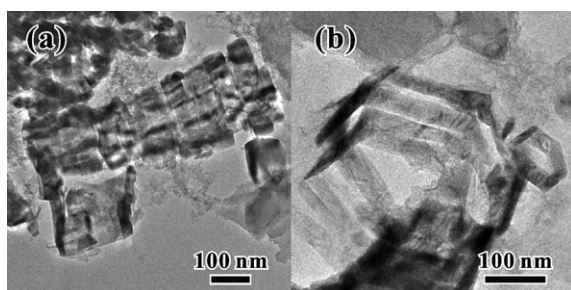
Fig. 4 Low-magnification TEM images of various hexagonal ring-like nanostructures broken from tower-like SnO_2 nanotubes under intense ultrasonic treatment.

Fig. 5 Models of atoms arrangements on different crystal planes of SnO_2 and ZnO: (a) $(100)_{SnO_2}\|(0001)_{ZnO}$, (b) $(010)_{SnO_2}\|(01\bar{1}0)_{ZnO}$.

(about 200 nm) are clearly observed. From the corresponding partial enlarged image (Fig. 3e) of the area "e", it can be found that the side surface of the tubular wall exhibits gradually descending steps along the axial direction of the nanotube, which is consistent with the fact observed from the SEM images. In addition, the dark-field TEM image (Fig. 3f) shows that the contrast of the area (enclosed by the dashed circles) having high-density planar structural defects is obviously darker than that of other areas of the nanotube. This indicates that great structural stress remains in the walls during the growth of tubular SnO_2. Furthermore, we found that these tower-like SnO_2 tubular structures are easily broken into ring-like segments when they are subjected to lengthy intense ultrasonic treatment (Fig. 4a). As shown in Fig. 4b, these ring-like segments are hexagonal.

On the basis of the above structural characterization, we can find that all SnO_2 nanotubes synthesized by the epitaxial casting approach presented here are highly orientated along the [100] direction. It should be pointed out that such high orientation and resulting single-crystallinity originate from the special epitaxial relationship between SnO_2 walls and ZnO templates. As shown in Fig. 5a, wurtzite-type ZnO and rutile-type SnO_2 have certain crystallographic comparability between the $(0001)_{ZnO}$ and $(100)_{SnO_2}$ planes where oxygen atoms exhibit a hexagonal close packing (hcp) arrangement or a pseudo-hcp arrangement, respectively. At the same time, the interplanar distances in the $[001]_{SnO2}\|[2\bar{1}10]_{ZnO}$ direction are very similar, 3.19 Å for SnO_2 and 3.24 Å for ZnO, as shown in Fig. 5b. When SnO_2 grows on the side surfaces (*i.e.*, $\{10\bar{1}0\}$ planes) of ZnO hexagonal columns, the SnO_2 epitaxial layer prefers to grow along the lattice-matching direction (*i.e.*, $[001]_{SnO2}\|[2\bar{1}10]_{ZnO}$) and enclosed ZnO nanorods to form close and single-crystalline rings.[23a] However, the lattice mismatch in the other growth direction (*i.e.*, $[100]_{SnO2}\|[0001]_{ZnO}$) is very large (up to 8.8%), and thus high-density structural defects are inevitably introduced to release the structural stress. This also accounts for the formation of stepped structures appearing in the tower-like SnO_2 nanotubes and hexagonal ring-like segments under lengthy intense ultrasonic treatment. Therefore the lattice-mismatch between ZnO and SnO_2 is the intrinsic factor for the growth of the SnO_2 epitaxial layer on the surface of the ZnO templates with different shapes and sizes. Besides that, the size and shape of the ZnO template as well as the deposition conditions (*i.e.*, flow rate, deposition time and temperature) of SnO_2 also have a great influence on the growth of the SnO_2 epitaxial layer because these extrinsic factors
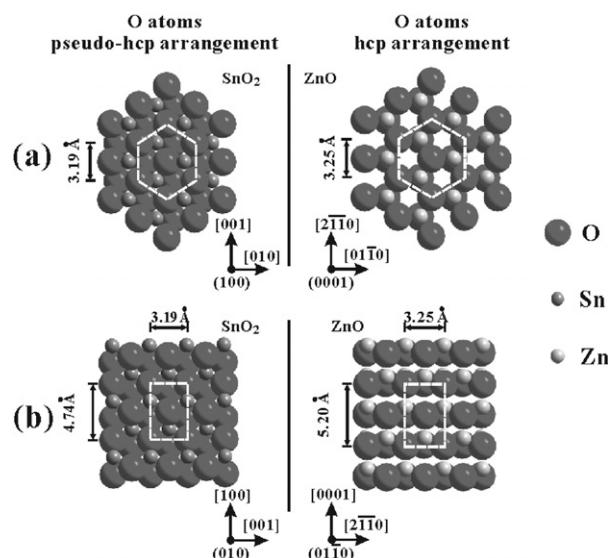
would influence the migration and nucleation of vapor atoms on the substrate.

Because the growth of the SnO_2 epitaxial layer depends on the supply of the precursor SnH_4, the wall thickness of SnO_2 nanotubes becomes tunable by simply controlling the experimental conditions during SnO_2 deposition. Fig. 6a is a typical SEM image of freestanding SnO_2 nanotubes prepared by using a rod-like ZnO array as the sacrificial template. In this case, the deposition process of SnO_2 lasted only 2 min. The walls of as-prepared tubular structures are so thin, about 20–30 nm, that they seem transparent under irradiation with the electron beam, and cannot vertically stand on the Si substrate after removing the ZnO array template. When simply prolonging the deposition time of SnO_2 to 15 min, well aligned SnO_2 nanotubes with thicker walls (200–250 nm) are successfully fabricated (Fig. 6b). Accordingly, the change in wall thickness of SnO_2 nanotubes along with the deposition time is reflected by the XRD pattern (see Fig. S2 in ESI‡). Visible broadening of diffraction peaks can be observed in the XRD pattern of SnO_2 nanotubes obtained *via* a deposition time of 2 min, implying small grain sizes of particles constructing tubular walls. According to the Scherrer equation, the average grain size is calculated to be about 23 nm, well consistent with the results from SEM observation. However,
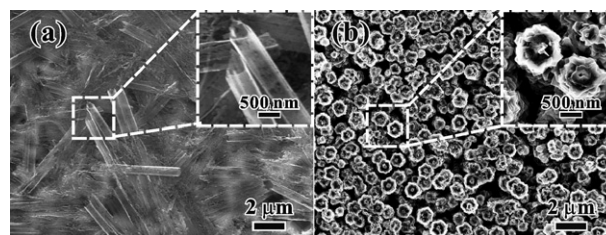

Fig. 6 Typical SEM images of SnO_2 nanotubes with different thicknesses prepared by using rod-like ZnO arrays as the sacrificial templates. The deposition times of SnO_2 were (a) 2 min and (b) 15 min. The insets are corresponding partial enlarged images.

XRD diffraction peaks of the as-synthesized SnO_2 nanotubes produced *via* a deposition time of 15 min become very narrow and sharp, indicating the increase of the size of SnO_2 crystallites when the tube walls become thicker.

Conclusions

In summary, various SnO_2 nanotube arrays have been successfully synthesized by using various pre-synthesized ZnO arrays as sacrificial templates. In comparison with previous SnO_2 nanotubes synthesized by porous membrane assisted sol–gel methods, our as-synthesized SnO_2 nanotubes not only are of single crystal-like structure, but also are able to orderly align on the substrates. More importantly, the construction forms and the wall thickness of these SnO_2 nanotubes can be tuned by simply selecting the appropriate ZnO templates and controlling the experimental conditions of SnO_2 deposition. Considering their special hollow structure and ordered arrangement, we believe that these as-synthesized SnO_2 nanotube arrays have potential applications in nanodevices, for example enhancing the response sensitivity of SnO_2-based sensors and the electrochemical performance of lithium batteries.

Acknowledgements

References

1 (*a*) W. Z. Li, C. H. Liang, J. S. Qiu, W. J. Zhou, H. M. Han, Z. B. Wei, G. Q. Sun and Q. Xin, *Carbon*, 2002, **40**, 787; (*b*) Q. Kuang, S. F. Li, Z. X. Xie, S. C. Lin, X. H. Zhang, S. Y. Xie, R. B. Huang and L. S. Zheng, *Carbon*, 2006, **44**, 1166; (*c*) Y. Bing, Y. W. Ma, H. S. Tao, L. S. Yu, G. Q. Jian, X. Z. Wang, X. S. Wang, Y. N. Lu and Z. Hu, *J. Mater. Chem.*, 2008, **18**, 1713.

2 K. F. Zhang, D. J. Guo, X. Liu, J. Li, H. L. Li and Z. X. Su, *J. Power Sources*, 2006, **162**, 1077.

3 (*a*) S. J. Son, J. Reichel, B. He, M. Schuchman and S. B. Lee, *J. Am. Chem. Soc.*, 2005, **127**, 7316; (*b*) S. J. Son, X. Bai and S. B. Lee, *Drug Discovery Today*, 2007, **12**, 650.

4 (*a*) Z. G. Mao and S. B. Sinnott, *J. Phys. Chem. B*, 2001, **105**, 6916; (*b*) Z. H. Wang, G. A. Luo, J. F. Chen, S. F. Xiao and Y. M. Wang, *Electrophoresis*, 2003, **24**, 4181; (*c*) P. Kowalczyk, L. Brualla, A. Zywocinski and S. K. Bhatia, *J. Phys. Chem. C*, 2007, **111**, 5250.

5 M. G. Bellino, J. G. Sacanell, D. G. Lamas, A. G. Leyva and N. E. W. De Reca, *J. Am. Chem. Soc.*, 2007, **129**, 3066.

6 (*a*) X. Wang, X. M. Sun, D. P. Yu, B. S. Zou and Y. D. Li, *Adv. Mater.*, 2003, **15**, 1442; (*b*) X. Wang and Y. D. Li, *Chem. Lett.*, 2004, **33**, 48; (*c*) H. Deng, J. W. Wang, Q. Peng, X. Wang and Y. D. Li, *Chem. Eur. J.*, 2005, **11**, 6519; (*d*) Y. D. Li, X. L. Li, R. R. He, J. Zhu and Z. X. Deng, *J. Am. Chem. Soc.*, 2002, **124**, 1411.

7 (*a*) M. Nath, A. Govindaraj and C. N. R. Rao, *Adv. Mater.*, 2001, **13**, 283; (*b*) M. Nath and C. N. R. Rao, *J. Am. Chem. Soc.*, 2001, **123**, 4841; (*c*) M. Nath and C. N. R. Rao, *Angew. Chem. Int. Ed.*, 2002, **41**, 3451; (*d*) G. Gundiah, S. Mukhopadhyay, U. G. Tumkurkar, A. Govindaraj, U. Maitra and C. N. R. Rao, *J. Mater. Chem.*, 2003, **13**, 2118.

8 (*a*) N. Du, H. Zhang, B. D. Chen, X. Y. Ma and D. R. Yang, *Chem. Commun.*, 2008, 3028; (*b*) Y. F. Qiu and S. H. Yang, *Nanotechnology*, 2008, **19**, 265606.

9 (*a*) X. X. Li, F. Y. Cheng, B. Guo and J. Chen, *J. Phys. Chem. B*, 2005, **109**, 14017; (*b*) C. D. Bae, S. Y. Kim, B. Y. Ahn, J. Y. Kim, M. M. Sung and H. J. Shin, *J. Mater. Chem.*, 2008, **18**, 1362.

10 (*a*) Q. Kuang, Z. W. Lin, W. Lian, Z. Y. Jiang, Z. X. Xie, R. B. Huang and L. S. Zheng, *J. Solid State Chem.*, 2007, **180**, 1236; (*b*) Z. W. Lin, Q. Kuang, W. Lian, Z. Y. Jiang, Z. X. Xie, R. B. Huang and L. S. Zheng, *J. Phys. Chem. B*, 2006, **110**, 23007; (*c*) S. H. Zhang, Z. X. Xie, Z. Y. Jiang, X. Xu, J. Xiang, R. B. Huang and L. S. Zheng, *Chem. Commun.*, 2004, 1106.

11 (*a*) D. B. Kuang, Y. P. Fang, H. Q. Liu, C. Frommen and D. Fenske, *J. Mater. Chem.*, 2003, **13**, 660; (*b*) J. R. Ota and S. K. Srivastava, *Nanotechnology*, 2005, **16**, 2415.

12 (*a*) A. M. Schwartzberg, T. Y. Olson, C. E. Talley and J. Z. Zhang, *J. Phys. Chem. C*, 2007, **111**, 16080; (*b*) W. M. Shen, H. Wang, H. S. Peng, L. Nie, D. Y. Chen and M. Jiang, *Chem. Commun.*, 2007, 2360; (*c*) C. Y. Wu, S. H. Yu, S. F. Chen, G. N. Liu and B. H. Liu, *J. Mater. Chem.*, 2006, **16**, 3326.

13 Y. N. Xia, P. D. Yang, Y. G. Sun, Y. Y. Wu, B. Mayer, B. Gates, Y. D. Yin, F. Kim and H. Q. Yan, *Adv. Mater.*, 2003, **25**, 353.

14 (*a*) Q. Kuang, C. S. Lao, Z. Li, Y. Z. Liu, Z. X. Xie, L. S. Zheng and Z. L. Wang, *J. Phys. Chem. C*, 2008, **112**, 11539; (*b*) Q. Kuang, C. S. Lao, Z. L. Wang, Z. X. Xie and L. S. Zheng, *J. Am. Chem. Soc.*, 2007, **129**, 6070.

15 (*a*) Y. Wang, H. C. Zeng and J. Y. Lee, *Adv. Mater.*, 2006, **18**, 645; (*b*) H. Kim and J. Cho, *J. Mater. Chem.*, 2008, **18**, 771; (*c*) Y. Wang, J. Y. Lee and H. C. Zeng, *Chem. Mater.*, 2005, **17**, 3899.

16 (*a*) Y. L. Wang, X. C. Jiang and Y. N. Xia, *J. Am. Chem. Soc.*, 2003, **125**, 16176; (*b*) B. Wang, L. F. Zhu, Y. H. Yang, N. S. Xu and G. W. Yang, *J. Phys. Chem. C*, 2008, **112**, 6643; (*c*) G. X. Wang, J. S. Park, M. S. Park and X. L. Gou, *Sens. Actuators B*, 2008, **131**, 313; (*d*) T. Hamaguchi, N. Yabuki, M. Uno, S. Yamanaka, M. Egashira, Y. Shimizu and T. Hyodo, *Sens. Actuators B*, 2006, **113**, 852.

17 N. G. Park, M. G. Kang, K. S. Ryu, K. M. Kim and S. H. Chang, *J. Photoch. Photobio. A*, 2004, **161**, 105.

18 (*a*) Y. H. Chen, X. T. Zhang, Z. H. Xue, Y. C. Li, Y. B. Huang, Z. L. Du and T. J. Li, *Chin. Sci. Bull.*, 2005, **50**, 618; (*b*) W. Zhu, W. Z. Wang, H. L. Xu and J. L. Shi, *Mater. Chem. Phys.*, 2006, **99**, 127.

19 M. Lai, J. A. G. Martinez, M. Grätzel and D. J. Riley, *J. Mater. Chem.*, 2006, **16**, 2843.

20 (*a*) M. Knez, R. Scholz, K. Nielsch, E. Pippel, D. Hesse, U. Gösele and M. Zacharias, *Nanotechnology*, 2006, **17**, 5157; (*b*) Y. B. Li, Y. Bando and D. Golberg, *Adv. Mater.*, 2005, **17**, 1401.

21 J. Goldberger, R. R. He, Y. F. Zhang, S. Lee, H. Q. Yan, H. J. Choi and P. D. Yang, *Nature*, 2003, **422**, 599.

22 H. Zhang, D. R. Yang, X. Y. Ma and D. L. Que, *Nanotechnology*, 2005, **16**, 2721.

23 (*a*) Q. Kuang, Z. Y. Jiang, Z. X. Xie, S. C. Lin, Z. W. Lin, S. Y. Xie, R. B. Huang and L. S. Zheng, *J. Am. Chem. Soc.*, 2005, **127**, 11777; (*b*) J. W. Zhao, C. H. Ye, X. S. Fang, L. R. Qin and L. D. Zhang, *Cryst. Growth Des.*, 2006, **6**, 2643.

24 Y. Sun, G. M. Fuge and M. N. R. Ashfold, *Chem. Phys. Lett.*, 2004, **396**, 21.